

Thermodynamic Stability of Domain 2 of Epithelial Cadherin[†]

Alka Prasad, Nicole A. Housley, and Susan Pedigo*

Department of Chemistry and Biochemistry, University of Mississippi, University, Mississippi 38677

Received February 10, 2004; Revised Manuscript Received April 12, 2004

ABSTRACT: Cadherin is a cell adhesion molecule that participates in ordered calcium-dependent self-association interactions both between molecules on the same cell surface (cis-interactions) and on neighboring cell surfaces (trans-interactions). Cadherin is a transmembrane protein that has 3–7 independently folded β -barrel extracellular domains. Both types of self-association interactions are mediated through the most N-terminal domain (Domain 1). Although the structural nature of the trans-interactions is clear, the nature of the cis-interactions is ambiguous despite several high-resolution structural studies. From earlier studies, it is understood that for the trans-interactions to happen, cis-interactions are mandatory. Hence, our first steps are to study the energetic driving forces for the cis-interactions. We have simplified the approach by first examining participating extracellular domains individually. We report here our initial experiments into the stability of Domain 2 of E-cadherin (ECAD2). ECAD2 appears monomeric, according to results from mass spectrometry and sedimentation equilibrium studies. We report denaturation data from differential scanning calorimetric experiments, and temperature and denaturant-induced unfolding experiments monitored by circular dichroism. These studies give a unified picture of the energetics of ECAD2-folding and stability, for which ΔG° is 6.6 kcal/mol, T_m is 54 °C, ΔH_m is 90 kcal/mol, and ΔC_p is 1300 cal/Kmol. These parameters are independent of calcium up to 5 mM, indicating that ECAD2 does not bind calcium at physiological calcium levels.

Cadherins are a family of calcium binding cell-adhesion proteins. Members of the cadherin family of proteins are named based on the tissue type in which they predominate; Epithelial (E-), Neural (N-) and Placental (P-) cadherins are the classical examples. Each cadherin polypeptide has 5–7 independently folded, extracellular domains (Figure 1A), a single membrane-spanning region, and a C-terminal cytoplasmic domain that interacts with the actin cytoskeleton through catenins (1–3). E-cadherins play a fundamental role in establishing and maintaining cell polarity of epithelial cells and are therefore responsible for morphogenesis (4). Loss of E-cadherin expression is correlated with the invasive potential of tumor cells in a variety of human carcinomas (5–7).

Cadherins participate in calcium-dependent interactions each involving a separate surface of the cadherin molecule. In an ordered series of events, calcium ions bind at the interface between each pair of the extracellular domains changing the relative disposition of the domains (8). This is followed by cis-dimerization between cadherins on the same cell surface (9, 10). Subsequently, cadherin cis-dimers from adjacent cells interact to form higher order structures (tetramers or greater). These trans-interactions are the basis of adhesion between cells and require domain 1 (ECAD1), the most N-terminal extracellular domain (11, 12). Each of these interactions is represented schematically in Figure 1A. Specificity of trans-interactions is mediated by ECAD1, as

well (11, 13, 14). Recently, there have been several reports that trans-interactions require the participation of more than just ECAD1 (15, 16).

The molecular interactions at the dimerization interface have remained unclear despite several high-resolution structures. Initial solution (17, 18) and crystal structures (14, 19) agreed that the domains are 7-strand β -barrel structures (Figure 1B), with calcium ions binding at the interface between the domains. However, the crystal structures disagree upon the nature of the dimer interface. This discrepancy has been addressed in a number of additional structural studies that indicate a preference for one of the two original dimer interface structures (10, 20). However, this preferred model (hydrogen bonding mediated by waters) does not satisfactorily explain specificity of dimer interactions. There is also a troubling issue regarding the disposition of a critical tryptophan in position 2 of Domain 1 that remains unresolved (10, 14, 20, 21). One might expect that there is a paradigm describing both the nature of the dimer and tetramer interface for this family of proteins. Structural studies have not supplied all of the answers.

As an alternative to structural approaches, our laboratory is interested in the energetic underpinnings of the ordered equilibria in which cadherin participates, including folding,

* To whom correspondence should be addressed. Tel.: (662)915-5328. Fax: (662)915-7300. E-mail: spedigo@olemiss.edu.

[†] This work is based on research supported by the National Science Foundation under grant number MCB 0212669.

¹ Abbreviations: CD, circular dichroism; DSC, differential scanning calorimetry; ECAD2, epithelial-cadherin domain 2; HEPES, (N-2-hydroxyethyl)piperazine-N'-[2-ethanesulfonic acid]); IPTG, isopropyl -D-thiogalactoside; SEC, size exclusion chromatography; Tris, tris-(hydroxymethyl)aminomethane; DEAE, diethylaminoethyl; MWCO, molecular weight cut off; MALDI-TOF, matrix-assisted laser desorption/ionization-time-of-flight; ES-TOF, electrospray-time-of-flight; OD, optical density.

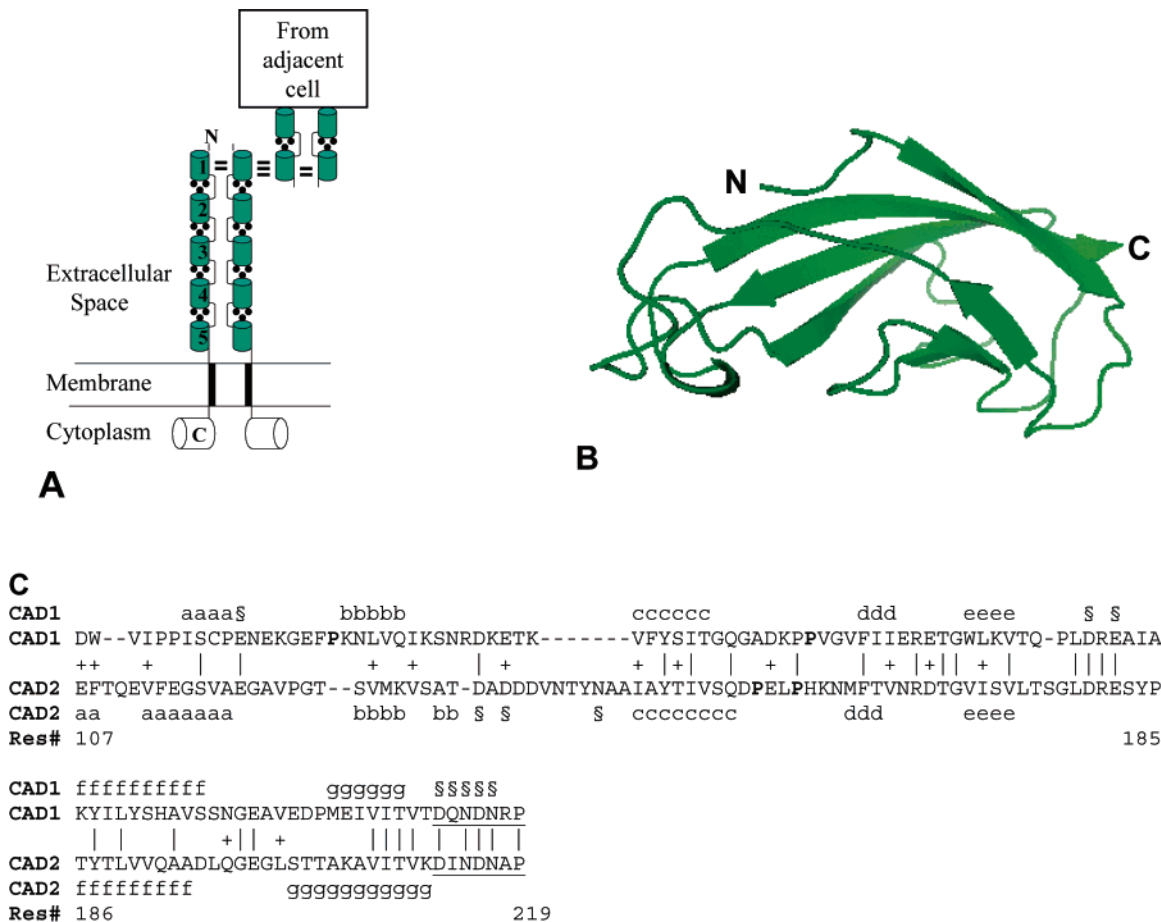


FIGURE 1: Representations of cadherin (ECAD): (A) A single ECAD polypeptide is represented from the N-terminal (N) extracellular barrel shaped domains numbered 1–5, a transmembrane segment (black bar), and a C-terminal domain (C) that is cytoplasmic. Up to 3 calcium ions (●) bind at the interface between the barrel-shaped extracellular domains forming the domain interface. Two ECAD molecules from the same cell surface interact in the presence of calcium to form the cis-dimerization interface. This is a face-to-face interaction denoted by the double bars (=). The trans-interaction occurs between ECAD dimers from adjacent cells oriented in an antiparallel fashion and is denoted by the triple bars (≡). (B) Ribbon drawing of backbone of residue for Domain 2 of E-cadherin (ECAD2; residues 107–212 of 1edh.pdb (19)). (C) The amino acid sequence of ECAD1 and ECAD2 are aligned to illustrate the regions of sequence similarity (28% identical and 41% similar). The linker regions are underlined. The cis X-Pro prolines are in bold. Residues that are identical (|) and similar (+) between the two domains are marked. The row preceding the ECAD1 sequence and following the ECAD2 sequence illustrate the residues that chelate the calcium ions in the interface between Domains 1 and 2 (\$) and the strand designations a–g for each domain according to PROCHECK analysis (35) of 1edh.pdb (19).

calcium binding, and dimerization. For over 4 decades, thermodynamics has been used to answer questions pertaining to protein folding, ligand binding to macromolecules, protein–protein interactions, and protein–nucleic acid interactions. Several critical examples of the utility of studies of the linkage between stability and ligand-binding follow. Lee and co-workers characterized the ligand-linked stability and assembly of cAMP Repressor Protein, a dimeric protein for which ligand binding is coupled to dimerization and association with DNA (see ref 22 and references therein). Ackers and co-workers have used the linkage between ligand binding and tetramer assembly in hemoglobin to characterize the existence of intermediate states in a process that was previously considered dominated only by the ligation end-states (see ref 23 and references therein). The issue of salt effects and linkage between stability and proton binding has been explored in several significant studies, including an initial proof of concept paper by Bolen and Santoro in which they demonstrated the linkage between pH, stability and protonation state of a derivative of chymotrypsinogen (24). More recently, a comprehensive study by McCrary et al. (25)

illustrated that discrepancies in DSC and spectroscopic approaches to stability measurements can be explained by anion and proton binding to Sac7d, a protein from the hyperthermophile *S. acidocaldarius*.

Our long-term goal is to resolve thermodynamic parameters for stability, binding of calcium, and dimerization of ECAD1 and ECAD2, both individually and linked. Results of these studies will be correlated with what is known regarding the function of protein in vivo. This paper focuses on developing an energetic profile of the stability ECAD2, the second extracellular domain of E-cadherin, in the presence and absence of calcium by using spectroscopic and calorimetric techniques.

EXPERIMENTAL PROCEDURES

Recombinant Plasmid Construction and Cloning. The original ECAD12 clone was provided by Dr. J. Engel (Biocenter, Basel, Switzerland) in pET-22b vector that coded for residues from 1 to 220 amino acids of the native protein from mouse epithelial cells (Domains 1 and 2). Primers for ECAD2 fragment were designed with the following consid-

erations. First, the left-hand primer was designed such that an NdeI restriction enzyme site was inserted before the codon for Glutamate 107 in the ECAD12 sequence. Second, the right-hand primer was designed such that a stop codon was added after the codon for Lysine 212 in the ECAD12 sequence. Third, a unique HindIII restriction enzyme site was added after the stop codon in the right-hand primer. Standard method of PCR amplification was conducted (www.stratagene.com) with Taq Polymerase and dNTPs for 30 cycles. The PCR product was purified using Standard Qiagen Kit, digested with NdeI and HindIII and ligated to pET-22b vector using T4 DNA ligase. Competent BL21 (DE3) cells were transformed with the ligation mix and plated on LB agar plates with 100 $\mu\text{g}/\text{mL}$ ampicillin. We screened for cell lines that expressed proteins of the correct molecular weight, purified the vector from those cell lines, and then sequenced the insert region of the vector to confirm its identity.

Overexpression and Purification. ECAD2 was overexpressed using the BL21 (DE3) expression cell line in 1-L volumes each inoculated with 5 mL of 50-mL overnight culture with 100 $\mu\text{g}/\text{mL}$ ampicillin. Cultures (1 L) were grown at 37 °C to OD_{600} of 1.0, then induced with 0.4 mM IPTG. Two hours post induction, the cells were harvested by centrifugation and frozen at -20 °C. Pellets from 1 L of culture were resuspended in 10–15 mL of 100 mM NaCl, 20 mM Tris/HCl, pH 7.4, then sonicated on ice for 2 min (2 s on, 2 s off). After centrifugation, ECAD2 was found in the soluble fraction.

ECAD2 was purified in two steps. A bulk fractionation was done to remove impurities. The soluble protein fraction was heat-treated at 80 °C for 10 min, cooled in ice for 5 min then centrifuged to separate the precipitated protein. ECAD2 remained in the soluble fraction. Additionally, the soluble protein fraction was purified chromatographically using DEAE-Sepharose Fast Flow Anion Exchange resin (Sigma) equilibrated with 100 mM NaCl, 20 mM Tris/HCl, pH 7.4. Protein was eluted in 300 mM NaCl, 20 mM Tris/HCl, pH 7.4, in a step gradient. Purity of protein was judged on Coomassie stained overloaded 17% SDS-PAGE to be > 95%. Protein was then dialyzed against 140 mM NaCl, 2 mM HEPES, pH 7.4, using Spectra/Por Membrane MWCO 8000. The molar absorptivity of native ECAD2 was determined to be 5120 $\text{M}^{-1}\text{cm}^{-1}$ at 278 nm (26).

Electrophoretic, Chromatographic, and Spectral Characterization. On the basis of migration on SDS-PAGE (Tris Glycine; 17%), as compared to Low Molecular Weight Standards (Sigma) the apparent molecular mass of ECAD2 was 15 600 Da. The calculated value based on the amino acid sequence was 11 362 Da, considering that the N-terminal methionine is not removed posttranslationally. A UV-scan of purified and dialyzed protein was taken on Cary 50 Bio UV-vis Spectrophotometer. CD data was acquired on a Model 202SF CD Spectrometer from 200 to 300 nm, with a 15 s averaging time. The protein concentration was approximately 10 μM with a path length of 2 mm in 2 mM HEPES, 140 mM NaCl, pH 7.4.

To explore the issue of homophilic associations, purified ECAD2 was chromatographed on Superose 12 (10/30; Pharmacia) in 10 mM potassium phosphate, 140 mM NaCl, pH 7.4. In preparation for mass spectral analysis, protein samples were dialyzed into water. These salt free samples

were analyzed by ES-TOF (University of Mississippi) mass spectrometry (negative mode). MALDI-TOF experiments were run at the Molecular Analysis Facility at the University of Iowa. The instrument was configured to run in positive mode with samples dissolved in 50/50 acetonitrile/0.1% Trifluoroacetic acid. The instrument was calibrated with lysozyme. All samples were run with α -cyano-4-hydroxycinnamic acid as the matrix.

Analytical Ultracentrifugation. Sedimentation Equilibrium experiments were performed using a Beckman Optima XLA analytical ultracentrifuge equipped with absorbance optics and an An60Ti rotor. The temperature was 24.71 °C as calibrated according to the procedure in Correia et al. (27). Experiments were done at 38 000 rpm with data collected at 278 nm at a spacing of 0.001 cm with nine averages in a step scan mode. Scans were collected from six solutions of ECAD2 that were initially 0.1 to 0.9 AU at 278 nm (20–180 μM). Equilibrium was checked by comparing scans at various times up to 12 h. Data sets were edited to contain only those regions within the cells and fit both jointly and independently with NONLIN (28, 29) (PC version supplied by Yphantis and Lary). NONLIN fits to an effective reduced molecular weight, σ , given by

$$\sigma = \frac{M(1 - \bar{v}\rho)\omega^2}{RT} \quad (1)$$

where M is the molecular weight, \bar{v} is the partial specific volume, ρ is the density of the solution, $\omega = 2\pi(\text{rpm})/60$, R is the gas constant, and T is the temperature in Kelvin (30). All experiments were done in 2 mM HEPES, 140 mM NaCl, pH 7.4. The density of the buffer was determined with an Anton Paar Density Meter DMA 5000 at 24.71 °C and found to be 1.003155 g/mL. The partial specific volume was calculated to be 0.7320 mL/g using SEDNTERP (J. Philo).

Unfolding Studies: Spectral Measurements. Temperature-Induced Unfolding. All CD experiments were performed on an AVIV 202SF Stopped Flow CD Spectrometer (Proterion). Wavelength scans of the protein and buffer were made before performing each unfolding experiment. The buffer was 2 mM HEPES, 140 mM NaCl, 20 μM EGTA, pH 7.4. The protein concentration was 5–20 μM . Scans were performed at a wavelength range of 200–300 nm at 25 °C. All CD experiments were done using a quartz cuvette with a path length of 1 cm with constant stirring of the cuvette solution.

For temperature-induced unfolding measurements, the cuvette was fitted with a screw top to prevent evaporation of the solution at high temperatures. The temperature probe was inserted through the cuvette screw top. Protein concentrations of 10 μM in 2 mM HEPES, 140 mM NaCl, pH 7.4 were used for all denaturation experiments. Unfolding measurements spanned a temperature range of 15–85 °C. The same samples were cooled back to 15 °C. The temperature ramp rate was set at 1 °C/min with data taken every degree. The equilibration time at each temperature was either 0 or 1 min. No difference in the resolved parameters was observed with the change in the scan rate. The acquisition time was 15 s. These values lead to an effective scan rate of 1 and 2 °C/min. All these measurements were taken at 216, 220, and 225 nm. Since there was no difference in the resolved parameters at these three wavelengths, we typically worked at 225 nm to increase the signal-to-noise ratio.

Temperature-induced denaturation of ECAD2 was also performed in the presence of 5 mM Ca²⁺. The rest of the experimental conditions were identical to those stated above.

Temperature-induced denaturation experiments were also performed in the presence of urea at concentrations 0.4, 0.8, 1.2, 1.6, 2.0, 2.4, and 2.8 M monitored at 225 nm with an equilibration time of 1 min. The unfolding transitions were fit to the Gibbs-Helmholz equation (eq 8 below). Resolved enthalpies and melting temperatures were fit to a linear equation. The slope yields and estimate of the ΔC_p of unfolding according to the Kirchoff's equation are shown below.

$$\Delta C_p = \frac{\delta \Delta H}{\delta T_m} \quad (2)$$

Urea-Induced Unfolding. Isothermal urea denaturation experiments were performed at four different temperatures 25, 30, 37, and 42 °C, using an automated titrimer. Urea was of ultrapure quality (Nacalai Tesque Inc, Kyoto, Japan). The concentration of urea stock solution was ~9 M, as calculated by measuring refractive index using a Bausch and Lomb Refractometer (31). CD signals were monitored at 216, 222, or 225 nm, with an equilibration time of 0 and 1.0 min and an averaging time of 15 s for each point.

Urea-induced denaturation of ECAD2 was also performed in the presence of 5 mM Ca²⁺ at 37 °C. The rest of the experimental conditions were identical to those stated above.

Unfolding Studies: Differential Scanning Calorimetry. ECAD2 stock (~380 μ M) was extensively dialyzed against 10 mM potassium phosphate, 140 mM NaCl, pH 7.4. Buffer was retained to dilute protein stock to 0.5 to 1.6 mg/mL (44 to 140 μ M). Protein was denatured in a Nano II DSC (Calorimetry Sciences Corp.) fitted with a capillary cell. All the samples were degassed for 2 min at room temperature prior to scanning by pulling a vacuum to approximately 5 mTorr. The scan rates were 1 and 2 °C/min. Samples were loaded on the fly after a buffer heating and cooling scan. The protein concentrations were determined by UV absorbance at 278 nm (5120 M⁻¹cm⁻¹) from baselines that were corrected for scattering.

Data Analysis. All data were analyzed using IGOR Pro (ver.4.0; Wavemetrics), with procedure files written in-house with the exception of the DSC data (see below). All data were analyzed according to a two-state unfolding model represented below as



and governed by the equilibrium constant K given in eq 4 for which $[U]$ is the concentration of the unfolded state and $[N]$ is the concentration if the native state at any point along the unfolding profile.

$$K = \frac{[U]}{[N]} = e^{-\Delta G/RT} \quad (4)$$

The mole fraction of unfolded species in a solution is given by eq 5.

$$f_u = \frac{K}{1 + K} \quad (5)$$

The f_u varies between 0 and 1 as the protein is unfolded and

must be corrected for the actual span and offset of the experimental data using the equation below, in which the span is the difference between the unfolded and native baselines, and the offset is the native baseline.

$$\text{signal} = f_u \cdot \text{span} + \text{offset} \quad (6)$$

For denaturant-induced unfolding, ΔG is given by

$$\Delta G = \Delta G^\circ - m_G[D] \quad (7)$$

where ΔG° is the stability of the protein in the absence of denaturant, and m_G is the sensitivity of the protein to denaturant (32, 33). Thus, the urea-induced denaturation experiments were fit with eqs 6 and 7.

Temperature-induced unfolding is governed by eq 8 shown below

$$\Delta G = \Delta H_m \left(1 - \frac{T}{T_m}\right) + \Delta C_p \left(T - T_m - T \ln \frac{T}{T_m}\right) \quad (8)$$

where ΔH_m is the enthalpy of unfolding at the melting temperature, T_m is the melting temperature, and ΔC_p is the heat capacity at the melting temperature. Thus, the temperature-induced denaturation experiments were fit to eqs 6 and 8.

All baseline parameters (simple linear equations) were floated when possible in fits to the spectral data. Exceptions are noted in the text or in figure legends. Thermodynamic parameters were floated simultaneously when possible. The temperature denaturation data required that the value of ΔC_p be fixed. In these fits, ΔC_p was constrained to values of 0, 0.5, and 1.0 kcal/Kmole. Convergence of fits to the temperature denaturation experiments required close guesses for the baseline parameters.

DSC data was processed in the following way: The program C_p calc provided with the Nano II DSC was used to convert the power readings into molar heat capacity using the concentration and molecular weight of the ECAD2, the volume of the cell, and the partial specific volume of 0.73 mL/g. These data were transferred into a program written by Dr. S. Edmondson (IgorDenat) (34) for IGOR Pro. The IgorDenat procedure module has flexibility in analysis, allowing for selection of an appropriate unfolding model, easy independent definition of both baselines, calculation of heat capacity from the baselines, simultaneous analysis of all parameters, and setting of the window over which data should be analyzed. The ratio of ΔH_{cal} to ΔH_m is a fitted parameter, β .

RESULTS

Sequence Gazing and Predictions. The studies reported here are focused on the second domain of E-cadherin without either of the adjoining linker regions. The amino acid sequences of ECAD1 and ECAD2 of E-cadherin were aligned to highlight the boundaries of the domains and linker regions (Figure 1C). From this alignment, we selected residue 107 (Glutamate) as the beginning of Domain 2. This residue is the first past the end of the consensus sequence for the linker region connecting Domains 1 and 2 (residues 100–106). The consensus sequence of the linker region is DXNDNXP (7 amino acid residues underlined in Figure 1C). The domain was continued through residue 212 (Lysine).

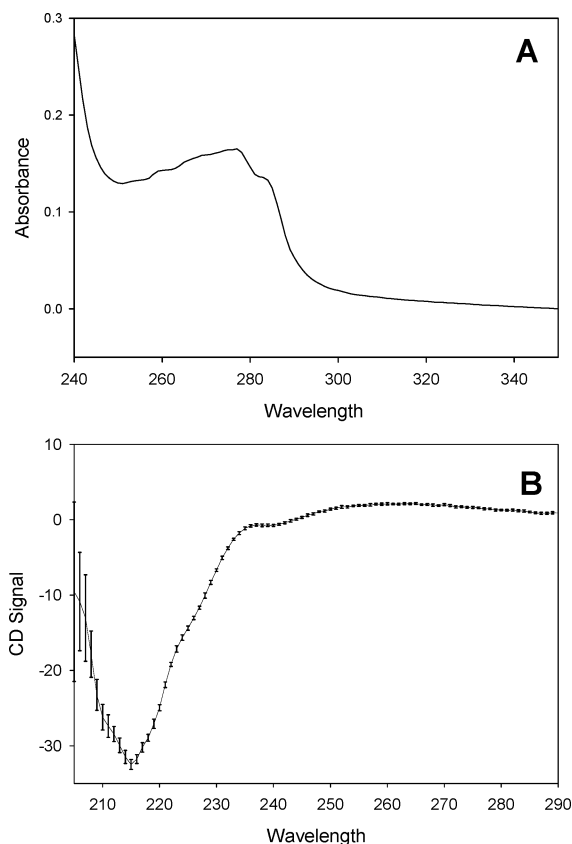


FIGURE 2: Spectral characterization of ECAD2: (A) UV-vis spectrum of ECAD2 at approximately $170 \mu\text{M}$ protein from 220 to 300 nm (0.2-cm path length, 2 mM HEPES, 140 mM NaCl, pH 7.4). (B) CD spectrum (in mdeg) of $10 \mu\text{M}$ ECAD2 from 205 to 290 nm (0.2-cm path length, 2 mM HEPES, 140 mM NaCl, pH 7.4).

This is the last residue before the beginning of the linker between Domains 2 and 3 (residues 213–219). (The consensus sequence of the end of the Domains 1 and 2 is VITVX.) We used PROCHECK (35) to define the regions of the protein that participate in the hydrogen bonding of the β -sheets (7 sheets per domain labeled a–g in Figure 1C) based on the structure by Nagar et al. (19) of the two domain construct. This program indicated that the crystallographic structure was consistent with our sequence alignment choices for the domain boundaries. Note that ECAD2 has 4 Prolines, 4 Tyrosines, no Cysteines, and no Tryptophans.

Spectral and Chromatographic Characterization. The UV-vis spectrum of the purified protein is shown in Figure 2A. One can see the low absorbance at 290 nm, confirming the absence of Tryptophan. The wavelength minimum in the CD spectrum (Figure 2B) is consistent with a predominantly β -sheet protein as expected from the crystallographic (10, 14, 19, 20) and solution structures (17, 18). Size exclusion chromatography of the purified protein revealed one large peak at approximately 19 000 Da in size. This peak was approximately 90% of the total peak area. There was also a small peak at the total excluded volume perhaps due to aggregated protein. Large molecular weight contaminants were not apparent in overloaded, Coomassie-stained SDS-PAGE gels.

Mass Spectrometry Experiments. The molecular ion peak from ES-TOF analysis of mass was 11 361 Da. These spectra were acquired in negative mode (ECAD2 has a charge of

negative 9 at pH 7.4 (SEDNTERP)). Alternatively, MALDI-TOF analysis of mass was 11 366 Da in positive mode. These values agree well with the molecular weight of 11 362 Da that is predicted from the sequence. Our concern over sample handling and ionization in mass spectrometric measurements led us to pursue additional confirmation that ECAD2 was monomeric.

Sedimentation Equilibrium Experiments. Equilibrium sedimentation experiments were conducted to confirm that ECAD2 is monomeric. Protein solutions varied in concentration from 20 to $190 \mu\text{M}$ (Figure 3). Global fits to the data in Figure 3 resulted in σ values of 1.853 (95% confidence interval is 1.805 to 1.901; $\sqrt{\text{var}} = 0.0087$). This yielded an estimate of the molecular weight of the protein between (10 907 Da best fit and range of 10 625 Da and 11 190 Da). This range fell slightly short of encompassing the actual molecular weight based on mass spectral data. The inset to Figure 3 shows that the molecular weight values resolved from analysis of individual data sets varied systematically with protein concentration indicating nonideality of the data, most likely due to a large charge-to-mass ratio for this construct (42). A linear fit to these data extrapolated to a y-intercept of $11\,420 \pm 320$ Da. This is very close to the expected value of 11 362 Da. These studies indicated that the ECAD2 protein was monomeric under these solution conditions.

Temperature-Denaturation. To characterize the thermodynamic parameters that govern the folding and stability of ECAD2, we used several different techniques, namely temperature- and urea-induced denaturation. First, ECAD2 was denatured using differential scanning calorimetry. A representative data set is shown in Figure 4A. For each data set, we resolved ΔH_m , T_m and ΔC_p simultaneously. Averages of the resolved values are reported in Table 1 for fits in which ΔC_p was floated. For each parameter, the standard deviation of the average is reported and is larger than the errors in parameters resolved from individual fits. These results are very similar to fits in which the value for ΔC_p was fixed at a value based on the extrapolation of the pre- and post-transition baseline. From these DSC experiments, the stability of the protein at 25 °C is 6.6 ± 1.2 kcal/mol. There was no scan rate (2-fold range) or concentration dependence (3-fold range) of resolved parameters. Refolding scans of these samples yielded exotherms with the same T_m but slightly smaller estimates for ΔH_m . The β -value resolved from these fits is 0.4 ± 0.1 .

We performed temperature denaturation of ECAD2 monitored by CD. These studies provided ΔH_m and T_m values by measuring a spectral signal and compliment the calorimetric experiments discussed above. A representative data set is shown in Figure 4B. The CD signal at 216, 220, 222 and 225 nm increased (became more negative) as the protein was denatured. Overlaid spectra at different temperatures do not demonstrate an isoelliptic point, but the wavelength range of spectra (215–300 nm) was limited in the far UV because of the path length of the sample cell. All data were fit to a two-state model according to eqs 6 and 8. The position and shape of the denaturation profile did not change with scan rate or wavelength that was monitored. ΔC_p was fixed at 0, 1, or 2 kcal/Kmol because all three parameters in eq 8 could not be simultaneously resolved. Resolved parameters for the fit with ΔC_p fixed at 1 kcal/Kmol are reported in Table 1.

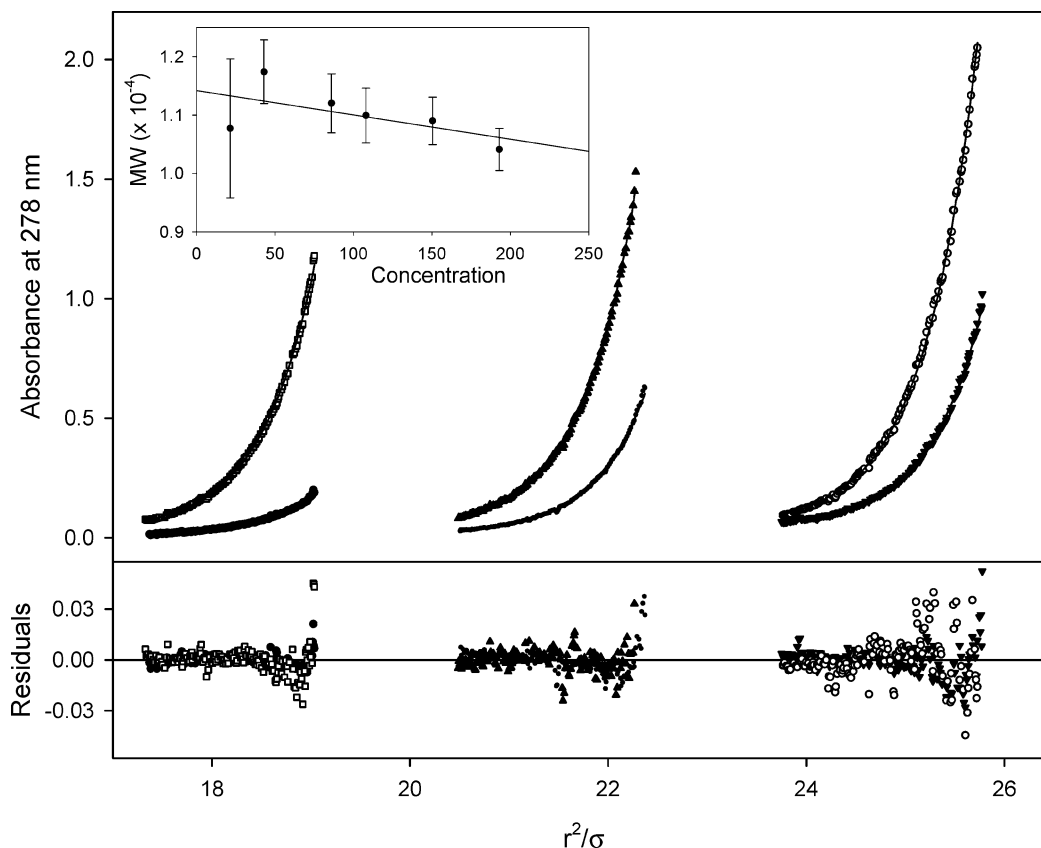


FIGURE 3: Sedimentation equilibrium data for ECAD2 at 38 000 rpm, 25 °C. Initial concentrations were 20 μM (\bullet), 40 μM (\circ), 80 μM (\blacktriangledown), 100 μM (\square), 140 μM (\blacktriangle), and 180 μM (\circ). Solid line illustrates results from a global fit of all six data sets to a monomer model. Residuals to global fits are shown in the lower panel. Inset: The apparent molecular weight resolved from fits to individual data sets is plotted versus the concentration of ECAD2 (μM) in the experiment. These data were fit to a line to resolve a y-intercept of $11\,420 \pm 320$ Da.

Table 1: Summary of Results from Analysis of Temperature Induced Denaturation Experiments

parameter	DSC ^a	CD ^b	urea + T_m ^c
ΔH_m (kcal/mol)	95 ± 6	89 ± 6	89 ± 1
T_m (deg C)	54.3 ± 0.5	54 ± 1	54.0 ± 0.1
ΔC_p (cal/Kmol)	1400 ± 800	$\langle 1000 \rangle$	1000 ± 100
ΔG deg (kcal/mol) ^d	6.6 ± 1.2	6.6 ± 0.5	6.6 ± 0.2

^a The value for ΔC_p was fixed at a value determined from the extrapolated pre- and post-transition baselines for fits for which all other parameters (baselines slope and intercept, T_m and ΔH_m) were floated. Value reported is the average value for 6 independent determinations. ^b Parameters resolved from fits to temperature-induced denaturation of ECAD2 monitored by change in CD signal. Values are averages of four determinations. Brackets indicate fixed parameters. ^c Results from fits of eq 8 to urea- and temperature-induced denaturation experiments. All parameters were floated. ^d Values calculated from eq 8.

From these temperature denaturation experiments, the stability of the protein at 25 °C is 6.6 ± 0.5 kcal/mol.

Temperature-induced denaturation in the presence of calcium produced a similar result as in the absence of calcium ($\Delta H_m = 80$ kcal/mol; $T_m = 55$ °C; $\Delta C_p = 1$ kcal/Kmol (fixed); data not shown). This indicates that the protein is not significantly stabilized by calcium.

Urea-Denaturation Experiments. We used urea-induced unfolding as an orthogonal method for determining the stability of the protein. This denaturation experiment was performed at 4 temperatures, 25, 30, 37, and 42 °C, as shown in Figure 5, which offered several advantages. First, the quality of the data at 25 °C was poor (The amplitude of the

signal was small due to the positive slope of the unfolded baseline.) Second, at higher temperatures, the unfolding curves were displaced to lower denaturant concentrations such that the amplitude of the signal was increased. Third, these data allowed broadening of the temperature range in Figure 6, which allowed resolution of ΔC_p from temperature denaturation data.

As can be seen in Figure 5, the CD signal of the protein increased as the protein unfolded as seen in the temperature-denaturation experiments. As the temperature increased, the midpoint of the transition moved to lower denaturant concentration, indicating that the protein was destabilized as temperature was increased. The slope of the unfolded baseline appears significant due to the small magnitude of the CD signal resulting from ECAD2, a predominantly β -sheet protein. There was a small bow in the unfolded baseline that led to systematic trends in the residuals plot. These data were fit to a two-state model according to eqs 6 and 7. Resolved parameters reported in Table 2 are for fits in which either the data sets were fit independently (individual m_G) or m_G was a global parameter (global m_G). Notice that the trend of the free energies and m -values is nonmonotonic when the m -value was not a global parameter. Although there is no basis for expecting m_G to be global, we would expect it to vary monotonically or over a shallow maximum over this temperature range (36). We believe that this nonmonotonic behavior does not result from a physically significant phenomenon, but rather is an artifact of analysis of data with such a small transition region.

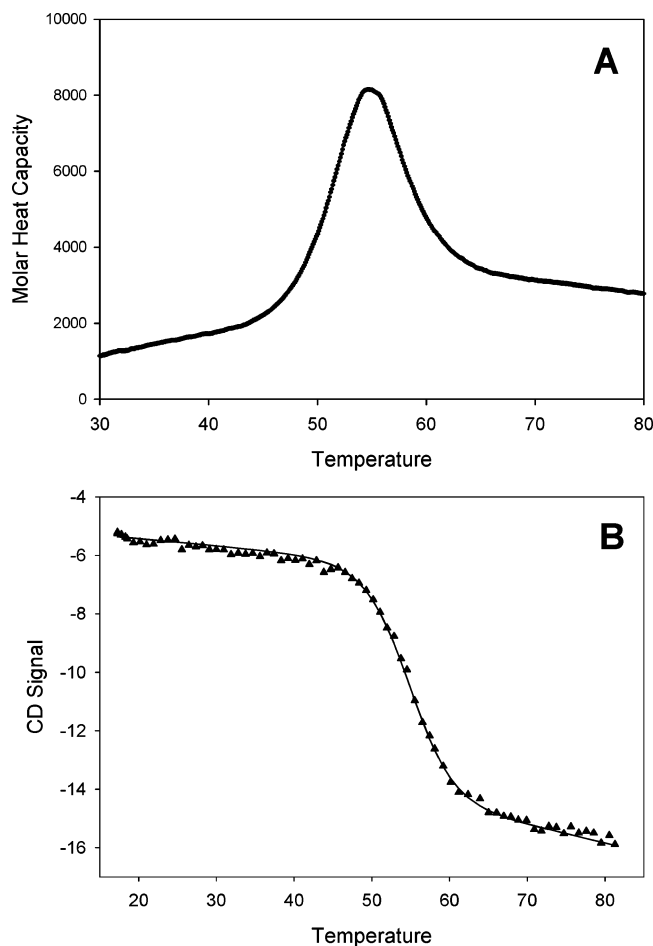


FIGURE 4: Representative data sets for the temperature denaturation of ECAD2: (A) Molar heat capacity (cal/Kmol) is plotted against the temperature ($^{\circ}\text{C}$) for the thermal denaturation of ECAD2 monitored by differential scanning calorimetry. Experimental conditions were as follows: protein concentration was 1.46 mg/mL; buffer was 10 mM potassium phosphate, 140 mM NaCl, pH 7.4; temperature range was from 15 to 80 $^{\circ}\text{C}$; scan rate was 1 $^{\circ}\text{C}/\text{min}$. Resolved parameters were $\Delta H_m = 99.8 \pm 0.1$ kcal/mol, $T_m = 54.2 \pm 0.1$ $^{\circ}\text{C}$ and $\Delta C_p = 1210 \pm 80$ kcal/Kmol. (B) CD signal at 225 nm (mdeg) is plotted against temperature ($^{\circ}\text{C}$) in an unfolding scan from 15 to 85 $^{\circ}\text{C}$ (\blacktriangle) with 0 min equilibration time. Solid line is simulated based on the following parameters $\Delta H_m = 82 \pm 2$ kcal/mol, $T_m = 55.0 \pm 0.1$ $^{\circ}\text{C}$ and $\Delta C_p = 1$ kcal/Kmol.

Urea-denaturation experiments at 37 $^{\circ}\text{C}$ were repeated at two different protein concentrations (5 and 50 μM) and in the presence of 5 mM CaCl_2 . There was no difference in the resolved free energies or m -values in these experiments as compared to those reported in Table 2. This indicates that ECAD2 does not bind calcium significantly at physiological concentrations (~ 1 mM), because it is not stabilized by calcium concentrations of 5 mM.

In Figure 6, the free energy changes from the urea-denaturation experiments were combined with those from the transition region of the temperature-denaturation experiments to provide a revised estimate of the enthalpy of unfolding and T_m . The extended temperature range afforded by the combined data set allowed resolution of ΔH_m , T_m and ΔC_p simultaneously, in fits to eq 8. Results are reported in Table 2. The value for ΔH_m and T_m were unchanged. The value resolved for ΔC_p was 1 kcal/Kmol, a similar value as that resolved from the DSC experiments. The free energy change at 25 $^{\circ}\text{C}$ was calculated to be 6.6 ± 0.2 kcal/mol.

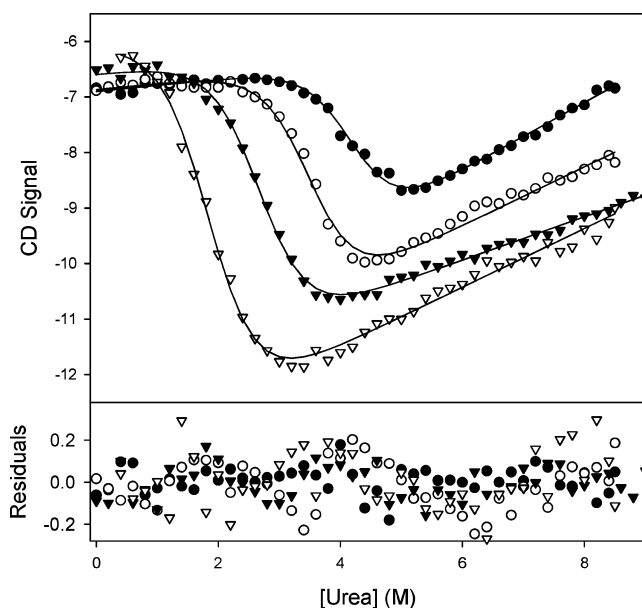


FIGURE 5: Urea denaturation of ECAD2 at four different temperatures. CD signal (mdeg; 225 nm) is plotted against the urea concentration (M) at 25 $^{\circ}\text{C}$ (\bullet), 30 $^{\circ}\text{C}$ (\circ), 37 $^{\circ}\text{C}$ (\blacktriangledown), and 42 $^{\circ}\text{C}$ (∇). Solid lines are simulated curves based on parameters resolved from global analysis of the data. The slope of the native baseline and the m_G value were global parameters. ΔG° , intercept of the native baseline, and the unfolded baseline were local parameters. All parameters except for the temperature and slope of the native baseline were floated. Resolved ΔG° and m_G values are reported in Table 2. Residuals of fits to data are shown.

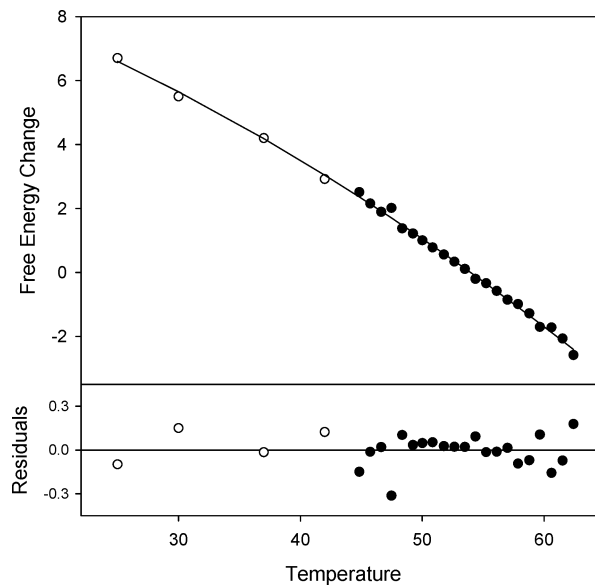


FIGURE 6: Combined urea- and temperature-denaturation data: Temperature-denaturation data (\bullet) reported in Figure 4B were baseline corrected, and data in the transition were converted to free energy using eq 5 and 6. Data from the urea-denaturation experiments (\circ) reported in Figure 5 were included. The combined data sets were fit to the Gibbs-Helmholtz equation to resolve enthalpy, change in heat capacity, and T_m as reported in Table 1. Residuals of fits to data are shown.

We also performed a series of temperature-denaturation experiments with low levels of urea present (Figure 7A) to determine ΔC_p , according to eq 2. The midpoint of the transition moved to lower temperature as the level of urea was increased (0–2.8 M urea in 0.4 M steps). Data were fit to the Gibbs-Helmholtz equation with ΔC_p fixed at 0.

Table 2: Summary of Results of Analysis of Urea-Denaturation Experiments

temp (deg C)	individual m_G^a		global m_G^b	
	ΔG deg (kcal/mol)	m_G (kcal/molM)	ΔG deg (kcal/mol)	m_G (kcal/molM)
25	6.0 ± 0.2	1.40 ± 0.06	6.7 ± 0.2	
30	6.6 ± 0.3	1.9 ± 0.1	5.5 ± 0.1	
37	4.1 ± 0.1	1.51 ± 0.05	4.2 ± 0.1	1.57 ± 0.04
42	2.8 ± 0.2	1.53 ± 0.08	2.9 ± 0.1	

^a All parameters were floated and local except for the slope of the native baseline. The native baseline was a global parameter fixed in these fits to the value resolved for the urea denaturation experiment at 25 °C. ^b All parameters were floated and local except for the slope of the native baseline and the m -value. The native baseline was a global parameter fixed in these fits to the value resolved for the urea denaturation experiment at 25 °C. The m -value was global and floated.

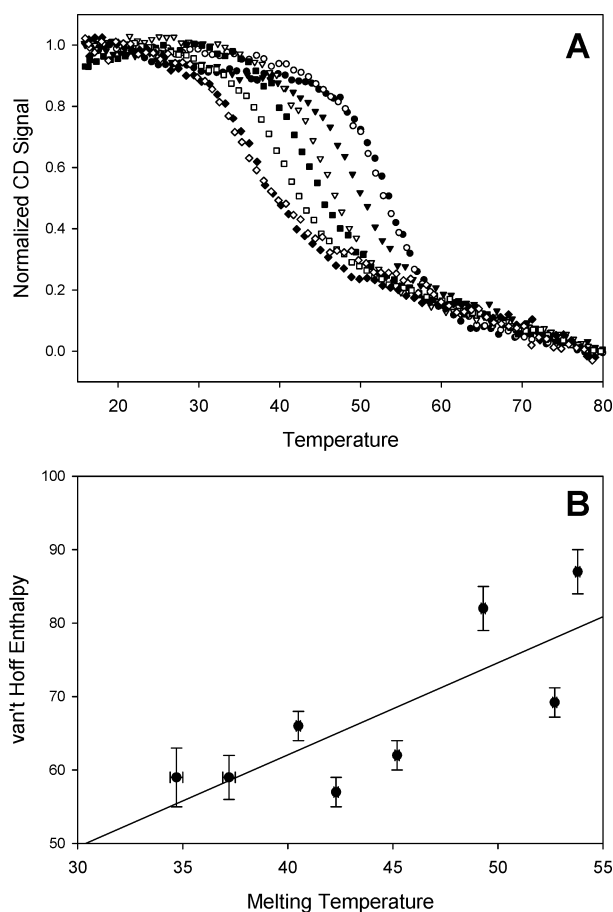


FIGURE 7: Temperature-induced unfolding of ECAD2 in the presence of urea. (A) Denaturation profiles for ECAD2 with 0 M (●), 0.4 M (○), 0.8 M (▼), 1.2 M (▽), 1.6 M (■), 2.0 M (□), 2.4 M (◆), and 2.8 M (◇) urea added. CD signals (mdeg) were normalized to represent the data on the same scale. (B) The van't Hoff enthalpy (kcal/mol) is plotted against the melting temperature (°C). Values were resolved from fits of the data in part A to the Gibbs-Helmholz equation in which ΔC_p was fixed to 0. Slope of the best-fit line to the data is 1.3 ± 0.4 kcal/Kmol.

Resolved values for ΔH_m and T_m were plotted (Figure 7B) and fit to a linear equation resolving an estimate of ΔC_p of 1.3 ± 0.4 kcal/Kmol. Note that these same samples were refolded (data not shown). Significant hysteresis was observed for solutions with urea added, such that the refolding was occurring at lower T_m than observed for the unfolding. As shown in Figure 1C, ECAD2 contains 2 cis X-Pro bonds.

The hysteresis could be due to a slow trans-cis isomerization that is observed only when the T_m is shifted to 50 °C or lower by addition of urea. We are exploring this phenomenon currently, and it is outside of the scope of the work reported here.

DISCUSSION

We study the linkage between calcium binding, stability, and cis-dimerization in cadherins. To that end, we must characterize the stability of each domain in isolation and in its molecular context, including neighboring domains and linker regions. It is important to begin dissection of this problem with a domain that neither dimerizes nor binds calcium. Our current focus has been on ECAD2 as a model domain to explore the intrinsic stability of extracellular domains of cadherins in the apo-state. The recombinant construct, ECAD2, lacks the adjacent linker regions. Because the majority of the calcium ligation occurs through associations with residues in this linker region, we did not expect it to bind calcium. Our experiments show that ECAD2 exists in a soluble and monomeric form in solution. Studies of this single domain protein are the first step toward identification of thermodynamic behavior of the whole molecule, ECAD12 in our case.

The Structure of ECAD2. ECAD domains have a similar topology to the immunoglobulin family (review of topology, ref 37), a 7-strand β -sheet protein with a Greek Key folding motif (see the Table of Contents graphic). In both solution and crystal structures of N- and ECAD1, all strands are antiparallel orientation except for strand A, which hydrogen bonds to strand B in an antiparallel fashion and to strand G in a parallel fashion (10, 14, 17, 19, 20). Crystal structures of ECAD2 are in the context of a two-domain construct (10, 19, 20). Alignment of sequences of Domains 1 (CAD1) and 2 (CAD2) in Figure 1C show that the greatest sequence similarity occurs in regions that contain calcium binding residues and regions that are hydrogen bonded in the β -sheet core of the protein. The greatest difference between the two domains is in the large connecting loops between strands and in the first strand segment in each domain (strand A). It is interesting that the strand A shows the least sequence similarity between the two domains. This segment is likely involved in the dimer interface, a phenomenon that apparently only ECAD1 participates in (14, 19, 38). Although domains 1 and 2 are only 28% identical, domains 2 through 5 are 70–85% identical (17), indicating that ECAD2 may be a reasonable model for the properties of domains 3, 4, and 5.

The CD scan showed that ECAD2 is primarily a β -sheet protein, consistent with structural studies of ECAD12 (19) and ECAD1 (17). The CD spectrum is very similar to others from predominantly β -sheet proteins such as a truncation mutant of Staphylococcal Nuclease (39) and for a 5-domain construct of cadherin (40). Interestingly, the CD signal increases (becomes more negative) as the protein unfolds (Figures 4B and 5). This has been observed at 234 nm for tryptophan-containing proteins (41) and also at 215 nm for proteins without tryptophan (42–44). The total signal change observed upon unfolding is small for β -sheet proteins.

We would like to draw attention to the fact that ECAD2 is monomeric according to mass spectrometric analysis of

Table 3: Summary of the Calculations of Total and Nonpolar Accessible Surface Area

	nonpolar ASA (Å ²)	total ASA (Å ²)
native	3228 ^a	6228 ^a
unfolded	9969 ^b	16911 ^c
difference	6471	10683

^a Refs 47 and 19. ^b Refs 48 and 49. ^c Ref 50.

its molecular weight, but appears to be approximately dimeric by size exclusion chromatography (SEC). We believe that this is due to the prolate ellipsoid shape of ECAD2, in which the one axis is twice the length of the other. Anomalous migration in SEC is important to note because several studies of the extracellular domains of cadherin report apparent sizes and draw conclusions about the dimeric state based on such experiments without comment regarding the pitfalls of interpretation of SEC experiments.

We confirmed the monomeric state of the protein through sedimentation equilibrium studies. Although the apparent molecular weight from those measurements (10 907 Da) is somewhat smaller than the actual molecular weight (11 362 D), there is no indication of a population of dimers. The sedimentation equilibrium studies were performed on samples of ECAD2 that spanned a concentration range over which the two domain construct would form dimers in the presence of calcium (45). Our results are similar to studies of dimerization of cadherin domains by Koch et al. (45).

Thermodynamics of Folding. Reversibility. The folding-refolding transition of ECAD2 is reversible. We recovered the initial CD signal after an unfolding then refolding cycle for each sample (data not shown). Second, UV-vis spectra of the protein solutions before and after DSC heating and cooling scans were found to be indistinguishable, indicating that the protein was recovered in a soluble form and not lost to insoluble aggregates. This was observed at all protein concentrations. Taken together, we believe that this indicates that the unfolding-refolding transition is reversible.

Heat Capacity Considerations. The change in heat capacity upon unfolding of ECAD2 was determined in several experiments, as reported in Table 1. In addition, we determined ΔC_p from a Kirchoff plot (Figure 7B), a method that usually yields reasonable estimates of ΔC_p (41, 46). The average experimental value for ΔC_p is 1.2 ± 0.8 kcal/Kmol.

Heat capacity change can be calculated based on the change in the solvent accessible surface area upon unfolding. The total accessible surface area of the protein in the folded state was calculated by *surface racer* (47), using a contrived pdb file created by deleting the coordinates for residues 1–106 and beyond residue 212, the calcium ions and waters and second B chain from 1EDH.pdb (19). The probe radius was 1.40 Å. The nonpolar accessible surface area was calculated by summing the areas for each amino acid according to the surface area values of Chothia (48, 49). The total accessible surface area was calculated by summing the areas for each amino acid according to the surface area values of Miller (50). Table 3 contains the nonpolar ($\Delta A_{np}SA$) and total accessible surface areas (ΔASA) for unfolded and native ECAD2. These values for ΔASA and $\Delta A_{np}SA$ agree well with values for other proteins of equivalent size (50, 51).

On the basis of these values for accessible surface area, we calculated ΔC_p and the m -value. Using the relationship

described by Livingstone et al., the value 6471 Å² for $\Delta A_{np}SA$ corresponds to a value of ΔC_p of 1.6 ± 0.3 kcal/Kmol (49). According to Myers et al., the value of 10 683 Å² for ΔASA corresponds to 2 kcal/Kmol. Using the relationship reported by Murphy and Freire, ΔC_p is 1.8 ± 0.2 kcal/Kmol (52). The average calculated value for ΔC_p is 1.80 ± 0.25 kcal/Kmol, which compares well to those resolved from experiments summarized in Table 1. It is possible that ECAD2 is not fully extended in the unfolded state leading to an overestimation of the accessible surface areas of the unfolded state and a calculated value for ΔC_p that is larger than the experimental value.

The values of ΔC_p that we report are those at T_m . We expect that the value of ΔC_p will be temperature dependent (53). However, the quality of our data is insufficient to indicate the magnitude of the dependence. We would have to discern curvature from the Kirchoff plot (54, 55), which clearly is not possible (Figure 7B).

ΔASA can also be used to estimate an m -value. According to Myers et al., the m -value in the urea experiments should be 1.54 kcal/molM (51). This value compares well to our value of 1.57 kcal/molM for the fits to the urea data, in which m_G was a global parameter (Table 2).

Free Energy, Enthalpy, and T_m . Because ECAD2 contains neither α -helix nor tryptophan, the magnitude of the CD signal change upon unfolding is small. Coupled with the uncertainty of the slope of the unfolded baseline, resolution of reliable parameters required the m -value to be made a global parameter (compare the parameter sets in Table 2). This is not optimal, but forced by the small magnitude of the transitions and the quality of the data at lower temperatures. We performed subsequent analysis for T_m , ΔH_m and ΔC_p (as reported in Figure 6), with the ΔG° and m -values from the individual analyses for the urea-denaturation experiments and obtained exactly the same parameters as reported in Table 2, except with slightly larger standard deviations.

Free energy change values determined from temperature-denaturation and urea-denaturation experiments agree within ~ 0.5 kcal/mol (see Tables 1 and 2) with the value from urea-denaturation studies being the lower value resulting from the two methods. The presence of urea can affect free energy estimates (56). However, our values agree well within their individual standard deviations.

Our data indicate that ECAD2 is quite stable even in the absence of its adjacent linker regions and bound Ca²⁺. This is interesting, given the relative instability of ECAD1 (data not shown). Most notably, we present data from three distinct methods, two spectroscopic and one calorimetric, that agree well with each other in terms of all resolved parameters (Tables 1 and 2). The thermodynamic parameters presented in Table 1 show that the accuracy of T_m values was within 1%, ΔH_m was within 5%, and ΔC_p was within 10%, consistent with the observations made for several two-state single domain proteins (46, 57) and giving confidence in our data.

ΔH_{cal} vs ΔH_m . Determination of ΔH_{cal} indicates that it is approximately half of ΔH_m . Experiments indicate that ECAD2 is monomeric, eliminating self-association as an explanation for the discrepancy. Preliminary sedimentation velocity experiments indicate that the protein stock contains a uniform distribution of species of a single molecular weight.

Table 4: Thermodynamic Parameters for Small Globular Proteins

protein	no. res	ΔH	ΔC_p	T_m	ΔG deg	m_G
Rnase Sa ^a	96	97.4	1.52	48.4	6.4	0.99
Rnase Sa3 ^a	96	93.6	1.57	47.2	5.9	1.05
Protein S (N-dom) ^b	88			68	5.0	1.2
Protein S ^b	173			43	3.6	1.9
SNase (V66W) ^c	136	28.1	0.81	47.5	1.87	2.12
β -lactoglobulin ^d	150	98.5		80.0	9.56	
Spect-SH3 ^e	62	44.9	0.69	63	3.25	
BTK-SH3 ^f	54	56		82	4.0	0.86
Fyn-SH3 ^g	67		0.86	72	6.0	1.36
RnaseT ₁ ^h		105.7	1.65	51.6	6.4	1.21

^a Ref 41 (Unreduced form of protein). ^b Ref 61. ^c Ref 39. ^d Ref 62. ^e Ref 63. ^f Ref 43 (Experiments in the presence of 500 mM Na₂SO₄. Free energy and m -value from denaturation experiments with Guanidinium HCl.). ^g Ref 64 (Denaturation experiments with Guanidinium HCl). ^h Ref 41 and references therein.

Thus, we do not believe that we have a heterogeneous population of species. It is possible that the domain is partially unfolded in the native state, consistent with the anomalously high apparent molecular weight by SEC. This would lead to a lower ΔH_{cal} and ΔH_m , but would not change their ratio. At this time, we do not have an explanation for the discrepancy. We plan to explore this further.

Thermodynamic Parameters of Other Small Globular Proteins. To resolve the structural and functional contradictions for the dimerization of cadherins, we plan to build a complete profile of all thermodynamic parameters of different relevant domains in the presence and absence of Ca²⁺. Predictions from one set of data would not be rational. However, the resolved set of parameters for individual domains should agree with data resolved for small proteins and the paradigms for protein folding (58–60). Table 4 contains a brief summary of the thermodynamic parameters for protein stability for small globular proteins that are predominantly β -sheet with the exception of RNase T₁. Relative to this group of proteins, ECAD2 appears to be stable and to have a high enthalpy change upon unfolding. This would be characteristic of a molecule for which there is a large change in hydrophobic surface area upon unfolding. High values for ΔH_m contrasted with the lower than predicted value for ΔC_p is problematic. The magnitude of these values should track for the same reasons. It is interesting to note that the thermodynamic parameters for unfolding of RNase T₁ are very similar to ECAD2. Like ECAD2, RNaseT₁ is an acidic protein; however, it is predominantly helical.

CONCLUSIONS

We presented studies that address the stability and thermodynamics of folding a small β -sheet protein, the second extracellular domain of cadherin. It was our goal to characterize this domain as a part of a larger puzzle of the energetics of the two domain constructs involving processes of folding, calcium binding, and dimerization. These studies reported here indicate that ECAD2 follows the general understanding of folding of globular proteins. This domain is quite stable even in the absence of calcium. It follows a two-state unfolding model. This construct exhibited similar thermodynamic properties both in the presence and in the absence of calcium. This indicates that calcium is not binding to ECAD2 perhaps due to the absence of the linker regions. It would also mean that calcium plays a significant role in

determining the conformation (dimerization) and function of the cadherin domain only when bound to its site on the protein and probably has no implications while present in a free state in the solution. Our data showed that even after eliminating the structural components necessary for calcium binding, we still have a stably folded domain. We consider ECAD2 the prototype for the repeating extracellular domains proximal to the membrane. It would be too early to predict the physiological implications on the whole protein (ECAD1-5 plus anchor and C-terminal domain, as shown in Figure 1A) just by looking at thermodynamic data from a single isolated domain. However, we can speculate that it is advantageous for cadherins to remain segregated into multiple folding units to accommodate (both structurally and functionally) exposure to different extracellular environments rather than to exist as a single globular protein. Perhaps multiple domains are important to their apparent function as spacers.

ACKNOWLEDGMENT

We would like to acknowledge Dr. J. Correia at the University of Mississippi Medical Center for help with the Sedimentation Equilibrium experiments, Ms H. Levanduski (UM) for assistance in cloning, and Dr. B. Watkins (UM; Department of Medicinal Chemistry) and Dr. L. Teesch (The University of Iowa, Molecular Analysis Facility) for mass spectra. Special thanks to Drs. M. Eftink, J. Correia and M. Mossing for advice and careful reading of the manuscript.

REFERENCES

- Kemler, R., and Ozawa, M. (1989) Uvomorulin–catenin complex: cytoplasmic anchorage of a Ca²⁺-dependent cell adhesion molecule, *Bioessays* 11, 88–91.
- Ozawa, M., Engel, J., and Kemler, R. (1990) Single amino acid substitutions in one Ca²⁺ binding site of uvomorulin abolish the adhesive function, *Cell* 63, 1033–1038.
- Takeichi, M. (1995) Morphogenetic roles of classic cadherins, *Curr. Opin. Cell Biol.* 7, 619–627.
- Boller, K., Vestweber, D., and Kemler, R. (1985) Cell-adhesion molecule uvomorulin is localized in the intermediate junctions of adult intestinal epithelial cells, *J. Cell Biol.* 100, 327–332.
- Birchmeier, W. (1995) E-cadherin as a tumor (invasion) suppressor gene, *Bioessays* 17, 97–99.
- Behrens, J. (1994) Cell contacts, differentiation, and invasiveness of epithelial cells, *Invasion Metastasis* 14, 61–70.
- Beavon, I. R. (1999) Regulation of E-cadherin: does hypoxia initiate the metastatic cascade?, *Mol. Pathol.* 52, 179–188.
- Pokutta, S., Herrenknecht, K., Kemler, R., and Engel, J. (1994) Conformational changes of the recombinant extracellular domain of E-cadherin upon calcium binding, *Eur. J. Biochem.* 223, 1019–1026.
- Tomschy, A., Fauser, C., Landwehr, R., and Engel, J. (1996) Homophilic adhesion of E-cadherin occurs by a cooperative two-step interaction of N-terminal domains, *Embo J.* 15, 3507–3514.
- Pertz, O., Bozic, D., Koch, A. W., Fauser, C., Brancaccio, A., and Engel, J. (1999) A new crystal structure, Ca²⁺ dependence and mutational analysis reveal molecular details of E-cadherin homoassociation, *EMBO J.* 18, 1738–1747.
- Nose, A., Tsuji, K., and Takeichi, M. (1990) Localization of specificity determining sites in cadherin cell adhesion molecules, *Cell* 61, 147–155.
- Amagai, M., Karpati, S., Prussick, R., Klaus-Kovtun, V., and Stanley, J. R. (1992) Autoantibodies against the amino-terminal cadherin-like binding domain of pemphigus vulgaris antigen are pathogenic, *J. Clin. Invest.* 90, 919–926.

13. Shan, W. S., Koch, A., Murray, J., Colman, D. R., and Shapiro, L. (1999) The adhesive binding site of cadherins revisited, *Biophys. Chem.* **82**, 157–163.
14. Shapiro, L., Fannon, A. M., Kwong, P. D., Thompson, A., Lehmann, M. S., Grubel, G., Legrand, J. F., Als-Nielsen, J., Colman, D. R., and Hendrickson, W. A. (1995) Structural basis of cell–cell adhesion by cadherins [see comments], *Nature* **374**, 327–337.
15. Chappuis-Flament, S., Wong, E., Hicks, L. D., Kay, C. M., and Gumbiner, B. M. (2001) Multiple cadherin extracellular repeats mediate homophilic binding and adhesion, *J. Cell Biol.* **154**, 231–243.
16. Sinaga, E., Jois, S. D., Avery, M., Makagiansar, I. T., Tambunan, U. S., Audus, K. L., and Siahaan, T. J. (2002) Increasing paracellular porosity by E-cadherin peptides: discovery of bulge and groove regions in the EC1-domain of E-cadherin, *Pharm. Res.* **19**, 1170–1179.
17. Overduin, M., Harvey, T. S., Bagby, S., Tong, K. I., Yau, P., Takeichi, M., and Ikura, M. (1995) Solution structure of the epithelial cadherin domain responsible for selective cell adhesion, *Science* **267**, 386–389.
18. Overduin, M., Tong, K. I., Kay, C. M., and Ikura, M. (1996) ¹H, ¹⁵N and ¹³C resonance assignments and monomeric structure of the amino-terminal extracellular domain of epithelial cadherin, *J. Biomol. NMR* **7**, 173–189.
19. Nagar, B., Overduin, M., Ikura, M., and Rini, J. M. (1996) Structural basis of calcium-induced E-cadherin rigidification and dimerization, *Nature* **380**, 360–364.
20. Tamura, K., Shan, W. S., Hendrickson, W. A., Colman, D. R., and Shapiro, L. (1998) Structure–function analysis of cell adhesion by neural (N-) cadherin, *Neuron* **20**, 1153–1163.
21. Koch, A. W., Bozic, D., Pertz, O., and Engel, J. (1999) Homophilic adhesion by cadherins, *Curr. Opin. Struct. Biol.* **9**, 275–281.
22. Lin, S. H., and Lee, J. C. (2002) Linkage of multiequilibria in DNA recognition by the D53H *Escherichia coli* cAMP receptor protein, *Biochemistry* **41**, 14935–14943.
23. Ackers, G. K. (1998) Deciphering the molecular code of hemoglobin allostery, *Adv. Protein Chem.* **51**, 185–253.
24. Bolen, D. W., and Santoro, M. M. (1988) Unfolding free energy changes determined by the linear extrapolation method. 2. Incorporation of ΔG degrees N–U values in a thermodynamic cycle, *Biochemistry* **27**, 8069–8074.
25. McCrary, B. S., Bedell, J., Edmondson, S. P., and Shriver, J. W. (1998) Linkage of protonation and anion binding to the folding of Sac7d, *J. Mol. Biol.* **276**, 203–224.
26. Gill, S. J., and von Hippel, P. H. (1989) Calculation of Protein Extinction Coefficients from Amino Acid Sequence Data, *Anal. Biochem.* **182**, 319–326.
27. Correia, J. J., Gilbert, S. P., Moyer, M. L., and Johnson, K. A. (1995) Sedimentation studies on the kinesin motor domain constructs K401, K366, and K341, *Biochemistry* **34**, 4898–907.
28. Johnson, M. L., Correia, J. J., Yphantis, D. A., and Halvorson, H. R. (1981) Analysis of data from the analytical ultracentrifuge by nonlinear least-squares techniques, *Biophys. J.* **36**, 575–588.
29. Johnson, M. L., and Frasier, S. G. (1985) Nonlinear least-squares analysis in *Methods in Enzymology* pp 301–342, Academic Press, New York.
30. Yphantis, D. A., and Waugh, D. F. (1956) Ultracentrifugal characterization by direct measurement of activity. I. Theoretical, *J. Phys. Chem.* **60**, 623–629.
31. Pace, C. N. (1986) Determination and analysis of urea and guanidine hydrochloride denaturation curves, *Methods Enzymol* **131**, 266–280.
32. Greene, R. F., Jr., and Pace, C. N. (1974) Urea and guanidine hydrochloride denaturation of ribonuclease, lysozyme, α -chymotrypsin, and β -lactoglobulin, *J. Biol. Chem.* **249**, 5388–5393.
33. Santoro, M. M., and Bolen, D. W. (1988) Unfolding free energy changes determined by the linear extrapolation method. 1. Unfolding of phenylmethanesulfonyl alpha-chymotrypsin using different denaturants, *Biochemistry* **27**, 8063–8068.
34. McCrary, B. S., Edmondson, S. P., and Shriver, J. W. (1996) Hyperthermophile protein folding thermodynamics: differential scanning calorimetry and chemical denaturation of Sac7d, *J. Mol. Biol.* **264**, 784–805.
35. Laskowski, R. A., MacArthur, M. W., Moss, D. S., and Thornton, J. N. (1993) PROCHECK: a program to check the stereochemical quality of protein structures, *J. Appl. Crystallogr.* **26**, 283–291.
36. Zweifel, M. E., and Barrick, D. (2002) Relationships between the temperature dependence of solvent denaturation and the denaturant dependence of protein stability curves, *Biophys. Chem.* **101–102**, 221–237.
37. Richardson, J. S. (1977) beta-Sheet topology and the relatedness of proteins, *Nature* **268**, 495–500.
38. Makagiansar, I. T., Nguyen, P. D., Ikesue, A., Kuczera, K., Dentler, W., Urbauer, J. L., Galeva, N., Alterman, M., and Siahaan, T. J. (2002) Disulfide bond formation promotes the cis- and trans-dimerization of the E-cadherin-derived first repeat, *J. Biol. Chem.* **277**, 16002–16010.
39. Eftink, M. R., Ionescu, R., Ramsay, G. D., Wong, C. Y., Wu, J. Q., and Maki, A. H. (1996) Thermodynamics of the unfolding and spectroscopic properties of the V66W mutant of Staphylococcal nuclease and its 1–136 fragment, *Biochemistry* **35**, 8084–8094.
40. Tong, K. I., Yau, P., Overduin, M., Bagby, S., Porumb, T., Takeichi, M., and Ikura, M. (1994) Purification and spectroscopic characterization of a recombinant amino-terminal polypeptide fragment of mouse epithelial cadherin, *FEBS Lett* **352**, 318–322.
41. Pace, C. N., Hebert, E. J., Shaw, K. L., Schell, D., Both, V., Krajcikova, D., Sevcik, J., Wilson, K. S., Dauter, Z., Hartley, R. W., and Grimsley, G. R. (1998) Conformational stability and thermodynamics of folding of ribonucleases Sa, Sa2, and Sa3, *J. Mol. Biol.* **279**, 271–286.
42. Menendez, M., Gasset, M., Laynez, J., Lopez-Zumel, C., Usobiaga, P., Topfer-Petersen, E., and Calvete, J. J. (1995) Analysis of the structural organization and thermal stability of two spermadhesins. Calorimetric, circular dichroic, and Fourier transform infrared spectroscopic studies, *Eur. J. Biochem.* **234**, 887–896.
43. Chen, Y. J., Lin, S. C., Tzeng, S. R., Patel, H. V., Lyu, P. C., and Cheng, J. W. (1996) Stability and folding of the SH3 domain of Bruton's tyrosine kinase, *Proteins* **26**, 465–471.
44. Bousquet, J. A., Garbay, C., Roques, B. P., and Mely, Y. (2000) Circular dichroic investigation of the native and non-native conformational states of the growth factor receptor-binding protein 2 N-terminal src homology domain 3: effect of binding to a proline-rich peptide from guanine nucleotide exchange factor, *Biochemistry* **39**, 7722–7735.
45. Koch, A. W., Pokutta, S., Lustig, A., and Engel, J. (1997) Calcium binding and homoassociation of E-cadherin domains, *Biochemistry* **36**, 7697–7705.
46. Pace, C. N., and Laurents, D. V. (1989) A new method for determining the heat capacity change for protein folding, *Biochemistry* **28**, 2520–2525.
47. Tsodikov, O. V., Record, M. T., Jr., and Sergeev, Y. V. (2002) A novel computer program for fast and exact calculation of accessible and molecular surface areas and average surface curvature, *J. Comput. Chem.* **23**, 600–609.
48. Chothia, C. (1976) The nature of the accessible and buried surfaces in proteins, *J. Mol. Biol.* **105**, 1–14.
49. Livingstone, J. R., Spolar, R. S., and Record, M. T., Jr. (1991) Contribution to the thermodynamics of protein folding from the reduction in water-accessible nonpolar surface area, *Biochemistry* **30**, 4237–4244.
50. Miller, S., Janin, J., Lesk, A. M., and Chothia, C. (1987) Interior and surface of monomeric proteins, *J. Mol. Biol.* **196**, 641–656.
51. Myers, J. K., Pace, C. N., and Scholtz, J. M. (1995) Denaturant *m* values and heat capacity changes: relation to changes in accessible surface areas of protein unfolding (published erratum appears in *Protein Sci.* 1996 5(5): 981), *Protein Sci.* **4**, 2138–2148.
52. Murphy, K. P., and Freire, E. (1992) Thermodynamics of structural stability and cooperative folding behavior in proteins, *Adv. Protein Chem.* **43**, 313–361.
53. Becktel, W. J., and Schellman, J. A. (1987) Protein stability curves, *Biopolymers* **26**, 1859–1877.
54. Chaires, J. B. (1997) Possible origin of differences between van't Hoff and calorimetric enthalpy estimates, *Biophys. Chem.* **64**, 15–23.
55. Privalov, P. L., Tiktopulo, E. I., Venyaminov, S., Griko, Yu V., Makhatadze, G. I., and Khechinashvili, N. N. (1989) Heat capacity and conformation of proteins in the denatured state, *J. Mol. Biol.* **205**, 737–750.
56. Johnson, C. M., and Fersht, A. R. (1995) Protein stability as a function of denaturant concentration: thermal stability of barnase in the presence of urea, *Biochemistry* **34**, 6795–6804.

57. Kumar, S., Tsai, C. J., and Nussinov, R. (2003) Temperature range of thermodynamic stability for the native state of reversible two-state proteins, *Biochemistry* 42, 4864–73.
58. Kauzmann, W. (1959) Some factors in the interpretation of protein denaturation, in *Advances in Protein Chemistry* (Anfinsen, J., C. B., Bailey, K., Edsall, J. T., and Anson, M. L., Eds.) pp 1–63, Academic Press, New York.
59. Tanford, C. (1968) Protein Denaturation, *Adv. Protein Chem.* 23.
60. Tanford, C. (1970) Protein Denaturation Part C. Theoretical models for the mechanism of denaturation, *Adv. Prot. Chem.* 24, 1–95.
61. Wenk, M., Baumgartner, R., Holak, T. A., Huber, R., Jaenicke, R., and Mayr, E. M. (1999) The domains of protein S from *Myxococcus xanthus*: structure, stability, and interactions, *J. Mol. Biol.* 286, 1533–1545.
62. Lapanje, S., and Poklar, N. (1989) Calorimetric and circular dichroic studies of the thermal denaturation of β -lactoglobulin, *Biophys. Chem.* 34, 155–162.
63. Viguera, A. R., Martinez, J. C., Filimonov, V. V., Mateo, P. L., and Serrano, L. (1994) Thermodynamic and kinetic analysis of the SH3 domain of spectrin shows a two-state folding transition, *Biochemistry* 33, 2142–2150.
64. Plaxco, K. W., Guijarro, J. I., Morton, C. J., Pitkeathly, M., Campbell, I. D., and Dobson, C. M. (1998) The folding kinetics and thermodynamics of the Fyn-SH3 domain, *Biochemistry* 37, 2529–2537.

BI049693C